Distance Dependent Model for the Delay Power Spectrum of In-room Radio Channels

Steinböck, Gerhard; Pedersen, Troels; Fleury, Bernard Henri; Wang, Wei; Raulefs, Ronald

Published in:
I E E E Transactions on Antennas and Propagation

DOI (link to publication from Publisher):
10.1109/TAP.2013.2260513

Publication date:
2013

Document Version
Accepted author manuscript, peer reviewed version

Distance Dependent Model for the Delay Power Spectrum of In-room Radio Channels

Gerhard Steinböck, Troels Pedersen, Bernard Henri Fleury, Wei Wang and Ronald Raulefs

***Abstract*—A model based on experimental observations of the delay power spectrum in closed rooms is proposed. The model includes the distance between the transmitter and the receiver as a parameter which makes it suitable for range based radio localization. The experimental observations motivate the proposed model of the delay power spectrum with a primary (early) component and a reverberant component (tail). The primary component is modeled as a Dirac delta function weighted according to an inverse distance power law (d^{-n}). The reverberant component is an exponentially decaying function with onset equal to the propagation time between transmitter and receiver. Its power decays exponentially with distance. The proposed model allows for the prediction of e.g. the path loss, mean delay, root mean squared (rms) delay spread, and kurtosis versus the distance. The model predictions are validated by measurements: they show good agreement with respect to distance dependent trends.**

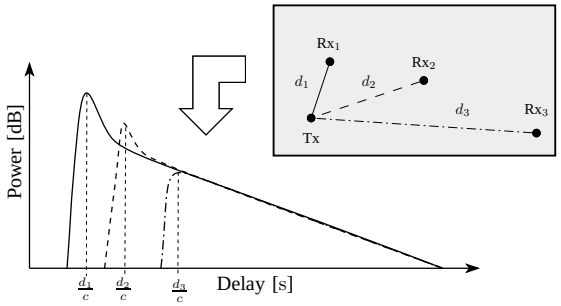

Fig. 1. Typical behavior of the bandlimited delay power spectrum experimentally observed at three different transmitter-receiver distances in an in-room environment (schematically presented by the grey box).

I. Introduction

Range based radio localization relies on models of the radio channel that incorporate distance as a parameter [1]. Such models allow for inferring on the transmitter-receiver distance from observations of range dependent channel features. For example currently deployed communication systems estimate the distance from the received signal strength based on a validated path loss model [1]. Wideband communication systems potentially allow for the exploitation of additional distance dependent information inherent in the dispersive behavior of the radio channel for localization purposes. Delay dispersion is characterized by means of the delay power spectrum, which is defined as the expectation of the squared impulse response. Thus, models describing the behavior of the delay power spectrum versus distance are in demand.

The delay power spectrum is a key component in wireless communications research of most stochastic models of the channel impulse response. The delay power spectrum is typically modeled as a one-sided exponentially decaying function of the delay [2]. Moreover, the power is normalized and the reference delay (origin) is selected to coincide with the onset delay. These transformations do not affect the bit error rate performance of communication systems operating in these stochastic channels, but the distance information potentially exploitable for localization is removed. Distance information is included in separate path loss models for an entire building [2]–[5] or for a single room [6]–[8] to perform coverage analysis.

We consider models for the in-room scenario as a basic element to cover entire buildings. Models of the delay power spectrum of in-room channels relying on reverberation theory, or room electromagnetics, have been recently proposed in [9]–[13]. These room electromagnetic models characterize the tail of the delay power spectrum, which is caused by reverberation, an effect similar to that occurring in room acoustics [14]. However, these models ignore the early part of the delay power spectrum, which is typically exploited for localization.

In the present contribution, the distance dependent model of the delay power spectrum is motivated by experimental observations [9], [11], [15] indicating that it exhibits an early, or primary, spike-like component followed by an exponential decaying tail. A model with a similar shape ("spike plus exponential tail") for outdoor scenarios was considered in [16] without including the distance dependence. The model proposed here consists of a primary and a reverberant component. The primary component is a Dirac delta function weighted according to an inverse distance power law (d^{-n}). The reverberant component is exponentially decaying with a distance-dependent onset and a reverberant field like behavior [11]. We denote the latter component as reverberant component, even though a reverberant field might not be entirely formed [9].

In this contribution, we extend the work presented in [17]. We derive the moment generating function and the kurtosis of the delay power spectrum. Additionally, a detailed investigation of the distance dependence of the primary and reverberant component is provided. This study leads to the concept of reverberation region. Furthermore, this contribution focuses on

Manuscript submitted March 2nd, 2012; revised December 8, 2012 and February 20, 2013; accepted March 26, 2013. This work was supported by the EU project ICT-248894 Wireless Hybrid Enhanced Mobile Radio Estimators 2 (WHERE2).

Gerhard Steinböck, Troels Pedersen and Bernard Henri Fleury are with the Dept. of Electronic Systems, Section Navigation and Communications at Aalborg University, Denmark. Wei Wang and Ronald Raulefs are with the Institute of Communications and Navigation, German Aerospace Center (DLR), Germany.

the validation of the model and uses additional experimental data in comparison to [17]. The relevance of the proposed delay power spectrum model is demonstrated by relating it to other published models and by means of two applications. These applications are a distance dependent model for the Rice factor and a time-discrete model to generate impulse responses.

The path loss prediction shows good agreement with the two distinct behaviors observed at both short and medium transmitter-receiver distances. So far this different behavior was not considered in path loss models, see e.g. [7] and references therein. We observe a good agreement between predicted values and estimates of the mean delay together with a predictable distance dependency, which is critical for localization purposes. The predicted and estimated values of the root mean squared (rms) delay spread are close with a distance behavior similar to that reported in [18], [19] for small to intermediate ranges.

II. Model of the Delay Power Spectrum

We consider an in-room environment as illustrated in Fig. 1 and assume that the wavelength is small compared to the smallest dimension of the room. The bandwidth of the considered system is assumed high enough to observe frequency fading (delay dispersion), but too low to separate single propagation paths in the environment.

We define the delay power spectrum as the expectation of the squared magnitude of the impulse response $h(\tau, d)$:

$$G(\tau, d) = \mathrm{E}[|h(\tau, d)|^2], \tag{1}$$

where τ is the delay and d is the transmitter-receiver distance. The expectation operator represents the mathematical abstraction of an averaging procedure to suppress variations due to small and large scale fading. This averaging procedure is used in [20] to obtain the so called long-term power delay profile. Realizations of $|h(\tau, d)|^2$ are sampled at different transmitter and receiver locations.

Fig. 1 illustrates the empirical observation that the delay power spectra in such an in-room scenario consist of an early part and a tail [9]–[11], [15]. The early part is strong at short distance and gradually vanishes as the distance increases and the tail has the same exponential decay[1] regardless of the transmitter-receiver distance.

We propose to model the delay power spectrum as a superposition of a primary and a reverberant component, each of which is distance dependent (see Appendix A):

$$G(\tau, d) = G_{\mathrm{pri}}(\tau, d) + G_{\mathrm{rev}}(\tau, d). \tag{2}$$

Subscript pri indicates the primary component and subscript rev the reverberant component. The primary component represents the early part of the delay power spectrum. It consists of the component resulting from direct propagation and possibly a superposition of components that may originate from first-order reflections on the floor, ceiling, and walls. We model the primary component as

$$G_{\mathrm{pri}}(\tau, d) = G_0 \left(\tfrac{d_0}{d}\right)^n \delta\left(\tau - \tfrac{d}{c}\right), \tag{3}$$

where n is the path gain exponent, $\delta(\,\cdot\,)$ is the Dirac delta function, c the speed of light, and $G_0 > 0$ is the gain at an arbitrary reference distance d_0. We chose the Dirac delta function as an approximation of the superimposed multipath components resulting from direct propagation and first order reflections as they cannot be resolved due to the bandwidth limitation.

The reverberant component is contributed by the multitude of higher order reflections in the room, which yield the tail in the measured delay power spectra. We model it as an exponentially decaying function with onset equal to the propagation time between the transmitter and receiver:

$$G_{\mathrm{rev}}(\tau, d) = \begin{cases} G_{0,\mathrm{rev}}\, e^{-\tau/T}, & \tau > \frac{d}{c} \\ 0, & \text{otherwise,} \end{cases} \tag{4}$$

where $G_{0,\mathrm{rev}}$ is the reference gain of the reverberant component. In analogy to room acoustics [11], [14] we term T the reverberation time.

The assumed exponential decay in (4) is inspired from experimental observations from literature [9]–[11], [15]. Reverberation theory [11], [13], [14], [21] predicts an exponentially decaying tail that exhibits a behavior with distance similar to (4). However, there may be other propagation phenomena leading to such an exponential decay. In this contribution we do not validate if the tail is created by reverberation; instead we rely only on experimental evidence to model the tail. Reverberation theory provides counterparts to some of the parameters that we use in the following sections. Therefore we use a terminology inspired by reverberation theory.

We will see in the following sections that the model (2)–(4) allows for the derivation of secondary models characterizing the behavior versus distance of narrowband parameters, like path loss and K-factor, and wideband parameters, like mean delay and rms delay spread.

TABLE I
Parameters of the proposed model.

Parameter	Meaning
G_0	Path gain at reference distance d_0.
d_0	Reference distance, typically 1 m.
n	Path gain exponent.
R_0	Ratio $G_{\mathrm{rev}}(d_0)/(G_{\mathrm{pri}}(d_0) + G_{\mathrm{rev}}(d_0))$.
T	Reverberation time.

A. Path Gain and Path Loss

The average path gain at distance d is obtained by integration of the delay power spectrum (2) with respect to delay:

$$G(d) = \int G(\tau, d)\, \mathrm{d}\tau, \tag{5}$$

$$= \underbrace{G_0 \left(\tfrac{d_0}{d}\right)^n}_{G_{\mathrm{pri}}(d)} + \underbrace{G_{0,\mathrm{rev}}\, T\, e^{\frac{-d}{c\,T}}}_{G_{\mathrm{rev}}(d)}. \tag{6}$$

[1] The theoretical investigations in [9] lead to a non-exponential tail, however some of the reported experimental results are close to exponential.

The component $G_{\mathrm{pri}}(d)$ decays as d^{-n}, while $G_{\mathrm{rev}}(d)$ decays exponentially. Note that the average path loss is defined as the inverse of the average path gain: $L(d) = G(d)^{-1}$. For mathematical convenience we consider the average path gain in the sequel and refer to it as path gain.

It is convenient to define a reverberation ratio $R(d)$ as the fraction of the total power contained in the reverberant component:

$$R(d) = \frac{G_{\mathrm{rev}}(d)}{G(d)}. \tag{7}$$

By definition $R(d)$ ranges from zero to unity. The introduction of the reverberation ratio simplifies the equations in the sequel. Furthermore, we chose to parameterize the model in terms of the reverberation ratio at the reference distance d_0, i.e. we recast (6) and (7) with $R_0 = R(d_0)$ as a parameter:

$$G(d) = G_0 \left(\tfrac{d_0}{d}\right)^n + G_0 \tfrac{R_0}{1-R_0}\, e^{\frac{d_0-d}{c\,T}}, \tag{8}$$

$$R(d) = \frac{1}{1 + \frac{1-R_0}{R_0}\left(\frac{d_0}{d}\right)^n e^{\frac{d-d_0}{c\,T}}}. \tag{9}$$

The parameter $R_0 \in [0, 1]$ indicates the balance between the primary and reverberant components at the reference distance. The ratio $\frac{1-R_0}{R_0}$ corresponds to the ratio of primary versus reverberant component ($G_{\mathrm{pri}}(d_0)/G_{\mathrm{rev}}(d_0)$) at the reference distance. The special case $R_0 = 0$, i.e. the reverberant component vanishes, leads to the "one-slope" model [4]

$$G(d) = G_{\mathrm{pri}}(d) = G_0 \left(\tfrac{d_0}{d}\right)^n. \tag{10}$$

This occurs when either $G_{0,\mathrm{rev}} = 0$ or the tail decays very fast, i.e. $T \approx 0$. In the other extreme where the primary component vanishes, i.e. $R(d) = R_0 = 1$, (8) simplifies to

$$G(d) = G_{\mathrm{rev}}(d) = G_{0,\mathrm{rev}}\, T\, e^{-\frac{d}{c\,T}}. \tag{11}$$

Blockage of the line-of-sight path will not lead to a vanishing primary component as the primary component may include additional first order reflections according to its definition.

Fig. 2a depicts example graphs of $G(d)$. For small distances d, the primary component dominates and the path gain decays as d^{-n}. For intermediate distances we observe a deviation from d^{-n} due to the reverberant component. For very large distances the influence of the reverberant component vanishes again.

B. Properties of the Reverberation Ratio

The reverberation ratio ranges by definition between zero and unity. In the following we derive properties of $R(d)$ under the assumption that $R_0 \neq 0$. We observe from (9) and Fig. 3 that $R(d)$ vanishes for very small and very large distances, where the primary component dominates the reverberant component. More specifically,

$$\lim_{d\to 0} R(d) = 0 \qquad \text{and} \qquad \lim_{d\to\infty} R(d) = 0. \tag{12}$$

For intermediate distances $R(d)$ approaches its maximum when the reverberant component dominates over the primary component. The distance $d_{\max}$ where $R(d)$ is maximum is obtained by differentiation of (9) and equating the result to zero:

$$d_{\max} = c\,T\,n. \tag{13}$$

At this distance the reverberation ratio is

$$R(d_{\max}) = \frac{1}{1 + \frac{1-R_0}{R_0} e^{-\frac{d_0}{c\,T}} \left(\frac{d_0\, e}{c\,T\,n}\right)^n}. \tag{14}$$

Notice that $d_{\max}$ only depends on n, T and c, the speed of light. The value $R(d_{\max})$ depends in addition on R_0 and d_0. It is less than unity except for the case $R_0 = 1$, i.e. when only the reverberant component is present. For the examples shown in Fig. 3, $d_{\max}$ is 12 m.

C. Mean Delay and Root Mean Squared Delay Spread

The mean delay is obtained from the delay power spectrum (2) as

$$\mu_\tau(d) = \frac{1}{G(d)} \int \tau\, G(\tau, d)\, \mathrm{d}\tau \tag{15}$$

$$= \tfrac{d}{c} + T\, R(d). \tag{16}$$

The first term in (16) is the delay of a directly propagating component and the second term results from the reverberant component. The mean delay is a function of the distance between transmitter and receiver and its value increases with distance. Fig. 2b depicts examples of the mean delay versus distance for different values of R_0. Using $R(d_{\max})$ and the upper bound of $R(d)$, which is unity, in (16), we can establish the following bounds for $\mu_\tau(d)$:

$$0 \leq \mu_\tau(d) \leq \tfrac{d}{c} + T\, R(d_{\max}) \leq \tfrac{d}{c} + T. \tag{17}$$

From the limits of $R(d)$ given in (12) and from (16) we conclude that

$$\lim_{d\to 0} \mu_\tau(d) = 0 \qquad \text{and} \qquad \lim_{d\to\infty} \mu_\tau(d) - \tfrac{d}{c} = 0. \tag{18}$$

Note that the distance range considered in the plot of Fig. 2b is too small to observe the convergence of $\mu_\tau(d)$ towards its asymptote $\frac{d}{c}$ for $d \to \infty$. The mean delay approaches $\frac{d}{c} + T$ for intermediate distances when $R(d)$ is close to unity.

The rms delay spread $\sigma_\tau(d)$ is computed as

$$\sigma_\tau^2(d) = \frac{1}{G(d)} \int \tau^2\, G(\tau, d)\, \mathrm{d}\tau - (\mu_\tau(d))^2 \tag{19}$$

$$= T^2 R(d)\,(2 - R(d))\,. \tag{20}$$

Hence the behavior of $R(d)$ determines that of $\sigma_\tau^2(d)$. Using (14) and the fact that $R(d)$ is unity in the case where there is only a reverberant component we obtain the following upper bounds:

$$\sigma_\tau^2(d) \leq T^2 R(d_{\max})\ (2 - R(d_{\max})) \leq T^2. \tag{21}$$

Furthermore, it can be seen from (12), that

$$\lim_{d\to 0} \sigma_\tau^2(d) = 0 \qquad \text{and} \qquad \lim_{d\to\infty} \sigma_\tau^2(d) = 0. \tag{22}$$

The rms delay spread is depicted as a function of distance in Fig. 2c. As for Fig. 2b the distance range considered in Fig. 2c is too small to observe the convergence of $\sigma_\tau(d)$ towards zero as d approaches infinity.

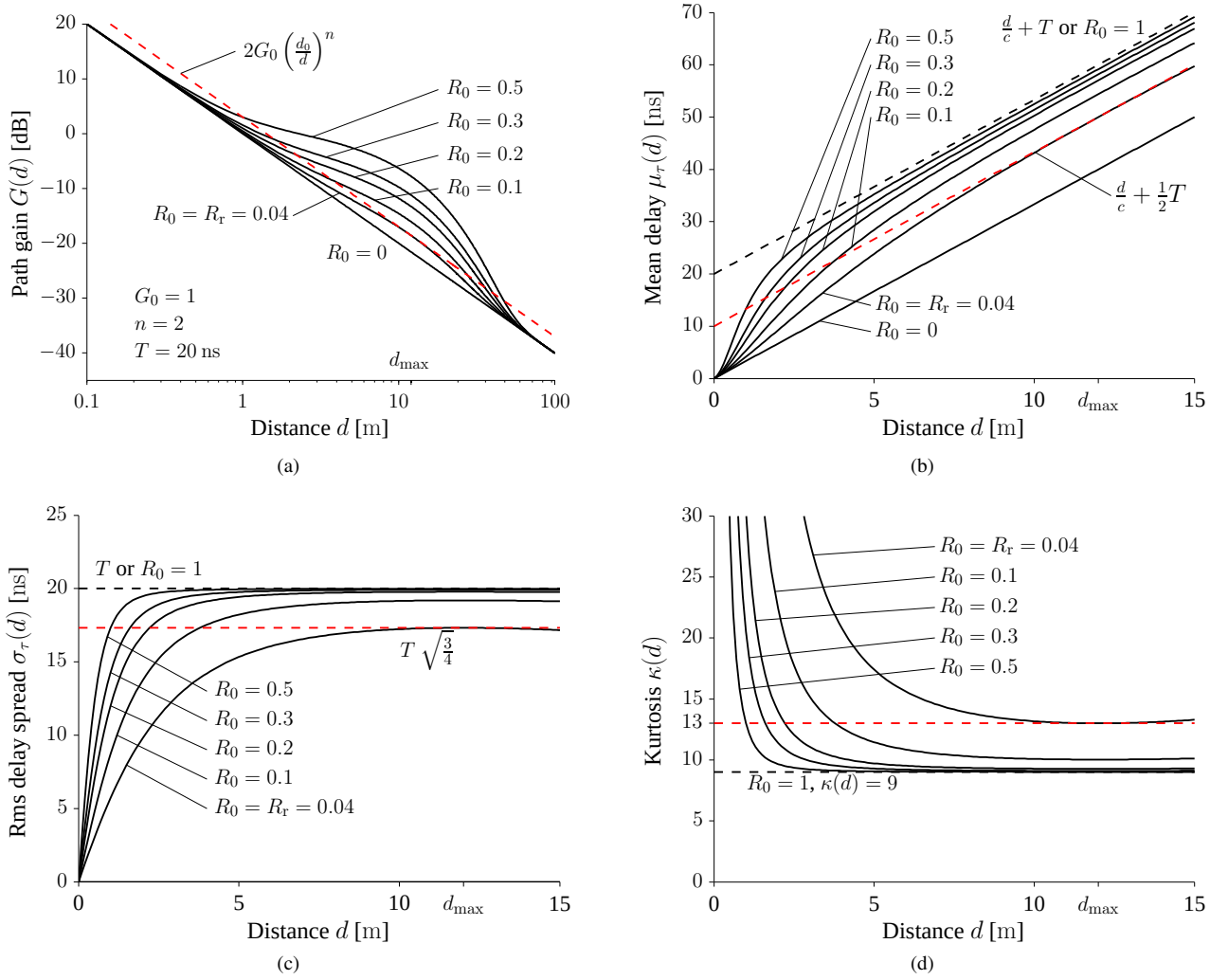

Fig. 2. Path gain (a), mean delay (b), rms delay spread (c) and kurtosis (d) versus distance predicted by the proposed model for $d_0 = 1$ m. The intersections of the various functions with the red dashed line mark the beginning and end of the reverberation region. The intersection at the end or the reverberation is not visible in (b), (c) and (d) due to chosen axis limitation. The reverberation region is observed if, and only if, $R_0 \geq R_\mathrm{r} = 0.04$ for these settings.

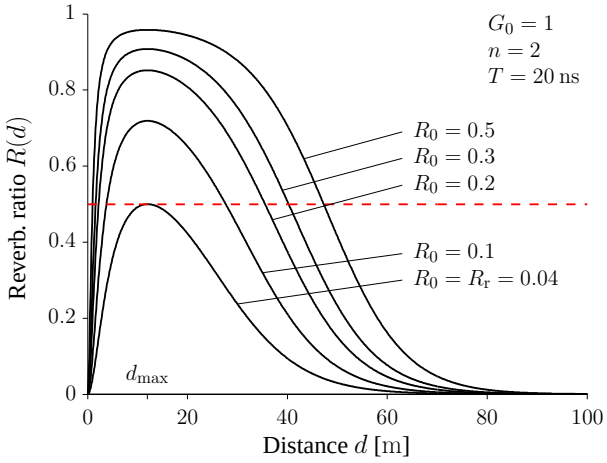

Fig. 3. Reverberation ratio versus the distance in linear scale. The intersections of $R(d)$ with the red dashed line mark the beginning and end of the reverberation region for the various parameter settings.

D. Centered Moment of Order k and Kurtosis

Analytical expressions for the centered moments of the delay power spectrum (2)–(4) are given in Appendix B. The third and fourth moments show similar dependency versus distance as the rms delay spread and therefore we omit presenting these results.

The kurtosis of $|h(\tau, d)|$ is used in localization to distinguish between line of sight or non-line of sight situations [22]–[26]. The kurtosis of the delay power spectrum is

$$\kappa(d) = \frac{\mu_4(d)}{\mu_2^2(d)}, \tag{23}$$

where $\mu_k(d)$ is the normalized kth centered moment of the delay power spectrum (55) derived in Appendix B. After inserting $\mu_2(d)$ and $\mu_4(d)$ in (23) we see that for small and large distances $\kappa(d)$ approaches infinity. For intermediate distances $\kappa(d)$ approaches its minimum value of nine, which coincides with the kurtosis of the exponential distribution [27]. Fig. 2d shows (23) for different settings of R_0.

We find the maximum of the moments of order $k \geq 2$ by equating the derivative of $\mu_k(d)$ to zero. Since these moments depend only on d via $R(d)$, we can write

$$\frac{\mathrm{d}\mu_k(d)}{\mathrm{d}d} = \frac{\mathrm{d}\mu_k(d)}{\mathrm{d}R(d)} \frac{\mathrm{d}R(d)}{\mathrm{d}d}. \tag{24}$$

The first factor in the right-hand product is positive, and therefore the root of (24) coincides with the root of the second factor, which is $d_{\max}$. Thus, all moments of order $k \geq 2$ attain their maximum value at distance $d_{\max}$. Furthermore, since $R(d) < 1$ we obtain

$$\mu_k(d) \leq T^k \sum_{\ell=0}^{k} \frac{k!}{\ell!} (-1)^{\ell} \qquad k \geq 2. \tag{25}$$

For $k = 2$, (25) combined with the identity $\sigma_\tau = \sqrt{\mu_2}$ yields the upper bound of the rms delay spread in (21).

E. Reverberation Region

For particular parameter values, it may occur that the power of the reverberant component equals or exceeds the power of the primary component at some distances, i.e. $G_{\mathrm{rev}}(d) \geq G_{\mathrm{pri}}(d)$ or equivalently $R(d) \geq \frac{1}{2}$. The reverberation region is the interval of distances for which $G_{\mathrm{rev}}(d) \geq G_{\mathrm{pri}}(d)$:

$$D_{\mathrm{rev}} = \{d \geq 0; R(d) \geq \tfrac{1}{2}\}. \tag{26}$$

The reverberation region is non empty if, and only if,

$$R_0 \geq \frac{1}{1 + e^{\frac{d_0}{c\,T}} \left(\frac{d_0\, e}{c\,T\,n}\right)^{-n}} = R_{\mathrm{r}}. \tag{27}$$

We define the reverberation distance as $d_{\mathrm{rl}} = \min D_{\mathrm{rev}}$. We consider the following three cases:

Case $R_0 < R_{\mathrm{r}}$: In this case the primary component is dominating over the reverberant component over all distances and D_{rev} is the empty set.

Case $R_0 = R_{\mathrm{r}}$: The reverberation region is a singleton: $D_{\mathrm{rev}} = \{d_{\max}\}$. In the graph of the path gain versus distance we observe a maximum of 3 dB deviation from $G_{\mathrm{pri}}(d_{\mathrm{rl}})$ (see Fig. 2a). We denote this largest possible reverberation distance $d_{\mathrm{rl,max}} = d_{\max}$. The parameter $d_{\mathrm{rl,max}}$ is of importance since it can be used for interpreting measurements: If the measured power does not exceed $G_{\mathrm{pri}}(d)$ by 3 dB at distances smaller than $d_{\mathrm{rl,max}}$, it will never occur. This result may be useful e.g. for the planning of in-room channel measurements.

Case $R_0 > R_{\mathrm{r}}$: In this case $D_{\mathrm{rev}} = [d_{\mathrm{rl}}, d_{\mathrm{ru}}]$, with $d_{\mathrm{rl}} < d_{\mathrm{ru}}$. The endpoints of the reverberation region are the two solutions of the identity $G_{\mathrm{pri}}(d) = G_{\mathrm{rev}}(d)$. After some algebraic manipulations this identity can be written as

$$-\frac{d_0}{c\,T\,n} \left(\frac{R_0}{1-R_0}\, e^{\frac{d-d_0}{c\,T}}\right)^{-\frac{1}{n}} = -\frac{1}{c\,T\,n}\, d\, e^{-\frac{1}{c\,T\,n} d}. \tag{28}$$

This expression can be solved in terms of the Lambert W function[2] [28]. For $z \in (-e^{-1}, 0)$, the Lambert W function provides two real solutions denoted by $W_0(z)$ and $W_{-1}(z)$),

[2]The Lambert W function is the (multi-valued) inverse of the complex function $w \mapsto w\, e^{w}$. For any complex number z, the values of $W(z)$ satisfy $z = W(z)\, e^{W(z)}$ [28].

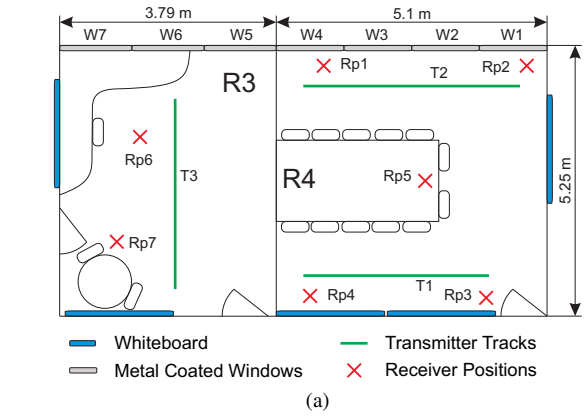

(a)

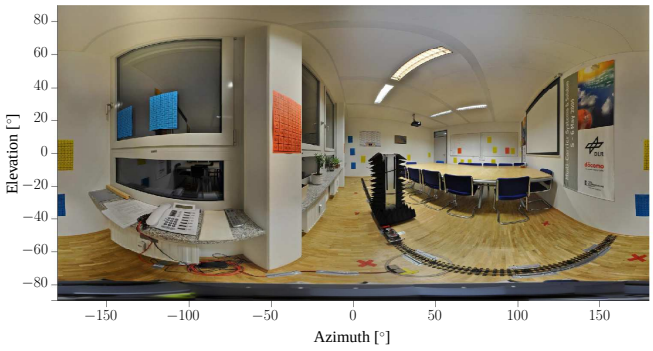

(b)

Fig. 4. Schematic of room R3 and R4 where the measurements were performed (a) and panograph (spherical panoramic photo) of R4 seen from Rp1 using an equi-rectangular projection (b).

respectively [28]. By inserting the left hand side of (28) for z in $W_0(z)$ we obtain

$$d_{\mathrm{rl}} = -c\,T\,n\,W_0\left(-\frac{d_0}{c\,T\,n}\left(\frac{R_0}{1-R_0}\, e^{\frac{d_0}{c\,T}}\right)^{-\frac{1}{n}}\right). \tag{29}$$

We obtain d_{ru} by replacing $W_0(\,\cdot\,)$ with $W_{-1}(\,\cdot\,)$ in (29).

We derive the following special values for the boundaries of the reverberation region:

$$\mu_\tau(d_{\mathrm{rl}}) = \tfrac{d_{\mathrm{rl}}}{c} + \tfrac{T}{2}, \tag{30}$$

$$\mu_\tau(d_{\mathrm{ru}}) = \tfrac{d_{\mathrm{ru}}}{c} + \tfrac{T}{2}, \tag{31}$$

$$\sigma_\tau(d_{\mathrm{rl}}) = \sigma_\tau(d_{\mathrm{ru}}) = T\sqrt{\tfrac{3}{4}}, \tag{32}$$

$$\kappa(d_{\mathrm{rl}}) = \kappa(d_{\mathrm{ru}}) = 13. \tag{33}$$

We see from (32) that $\sigma_\tau(d_{\mathrm{rl}})$ depends only on the reverberation time. We can use this result, together with an estimate of T, to estimate d_{rl} for a given room. To obtain an estimate of T from the rms delay spread one might simply average the rms delay spread estimates obtained for distances within an interval where these estimates show a constant trend. For the case that $R_0 \leq R_{\mathrm{r}}$ the maximum of the rms delay spread is $\max_{d\geq 0}\{\sigma_\tau(d)\} \leq T\sqrt{\frac{3}{4}}$ and, similarly, $\max_{d\geq 0}\{\mu_\tau(d) - \frac{d}{c}\} \leq \frac{T}{2}$.

F. Relation to Other Models and Measurements

The contributions [9], [11] investigate the delay power spectrum in reverberant environments. In [11] it is shown

that a diffuse field induces a delay power spectrum with an exponentially decaying tail. As shown in [9], the diffuse field occurs after an initial build up phase. The analysis in [9] indicates that the buildup phase lasts for so long that it cannot be neglected. This leads the authors to propose a model of the delay power spectrum with a non-exponentially decaying tail. The exponentially decaying tail in the model (2)–(4) is motivated solely by empirical observations. Therefore, the model is valid as long as (4) holds. A modification of (4) towards a non-exponential decay as in [9] is straightforward. Note that one of the two measurements in [9] is well described by an exponentially decaying tail.

Neither [9] nor [11] report the delay power spectrum in a form suitable to derive secondary models for path loss, mean delay, etc. versus distance. The model in [9] characterizes the delay power spectrum as a direct ray plus a non-exponential tail[3] for an average transmitter-receiver distance corresponding to the mean-free path[4] of the room. In [11] the early part of the delay power spectrum and the distance dependent onset of the tail are not specified. The way the models in [9], [11] are constructed hinders the derivation of secondary models. In contrast, the model (2)–(4) induces such secondary models (see (8), (16), and (20)).

Published measurements of the received power [29], [30] indicate a distinct behavior at short, intermediate and large distances. The decay of the total power versus distance, however, is commonly approximated with a one-slope model [7], [29], [30]. The approximation with a single path loss exponent leads to estimates of the path loss exponents smaller than the free space exponent and an overall poor model prediction. The path gain model in (8) mimics the difference in behavior at short, intermediate and large distances, as can be seen in Section II-A.

We introduce in Section II-E the new concept of reverberation region, where the reverberant component dominates. Furthermore, we define the reverberation distance to be the lower boundary of the reverberation region, cf. d_{rl} in (29). At this distance the primary and reverberant components have equal power, so our definition is in line with the classical definition of the reverberation distance or "effective radius" well known in room acoustics [14] and room electromagnetics [11], [31]. Note, however, that in our model, a second such distance might exist, namely d_{ru}, due to the fact that the power of the tail decays exponentially versus distance.

According to the model (20), the rms delay spread increases with distance up to the reverberation distance, stabilizes at a constant plateau within the reverberation region, and decreases outside the reverberation region. The empirical values of the rms delay spread reported in the survey [32] exhibit inconclusive behavior with respect to distance dependence: the rms delay spread is reported to both increase and decrease with distance. We conjecture that this behavior may be due to the used rms delay spread estimators. The measurements and results from ray-tracing simulations reported in [18], [19] agree with (20).

[3]More specifically, the direct ray and the tail's onset are both shifted to delay zero and the delay power spectrum is normalized such that the power of the direct ray is unity.

[4]In [9] the mean-free path is obtained as the product of the speed of light and the average number of wall reflections per second.

TABLE II
SETTING OF THE CHANNEL SOUNDER AND PARAMETERS FOR DATA POST-PROCESSING.

Sounder Settings	Value
Carrier frequency f_c	5.2 GHz
Bandwidth B	120 MHz
Number of sub-carriers N_c	1537
Carrier separation Δ_f	78.125 kHz
Signal duration T_{S}	12.8 µs
Cycle duration T_{C}	204.8 µs
Cycles per burst C	20
Burst duration T_{B}	4096 µs
Burst repetition time T_{BR}	131.072 ms
Transmit power	0 dBm
Delay MUX and cable τ_{mux}	3.86 ns
Number of receive antennas M	8
Post-processing Settings	
Threshold θ	-61 dB
Start delay range T estimator τ_{s} in R4	25 ns
Start delay range T estimator τ_{s} in R3	16.7 ns
End delay range T estimator τ_{max}	150 ns
Reference distance d_0	1 m

In summary, the model (2)–(4) of the delay power spectrum induces secondary models for the path gain, mean delay and rms delay spread etc. versus distance. These secondary models are interconnected via the initial model (2)–(4), in the sense that they share common parameters and are thus consistent. This consistency cannot be ensured when the models are derived independently from each other, as currently done in the literature. Our secondary models show good agreement with experimental data published in [7], [11], [18], [19], [29]–[32]. In the following two sections, we validate the model (2)–(4) by comparing the predictions achieved with the secondary models to measurements.

III. MEASUREMENT DATA

We validate the proposed model by means of measurement data from a campaign [33] conducted at the DLR premises in Oberpfaffenhofen, Germany. In the following we describe in detail the measurement campaign and the post-processing of the measurement data.

A. Measurement Campaign

Measurements were collected in a meeting room (R4) and an adjacent office (R3) depicted in Fig. 4. The dimensions of the R4 and R3 are $5.1\times5.25\times2.78\,\mathrm{m}^3$ and $3.79\times5.25\times2.78\,\mathrm{m}^3$, respectively. The inner walls are made of plaster boards. As visible in the panograph, the outer "wall" consists mainly of four windows (W1–W4) and two concrete pillars in R4. The office has only three windows (W5–W7). The window frames are metallic and the glass is metal coated. In both rooms the heights of the transmit and receive antennas were $1.26\,\mathrm{m}$ and $1.1\,\mathrm{m}$, respectively. The environment was static and no one was in the room while the measurements were taken.

The measurement data were collected using the Rusk-DLR channel sounder [34] operating at $5.2\,\mathrm{GHz}$. The transmitter and receiver were synchronized to a common Rubidium clock

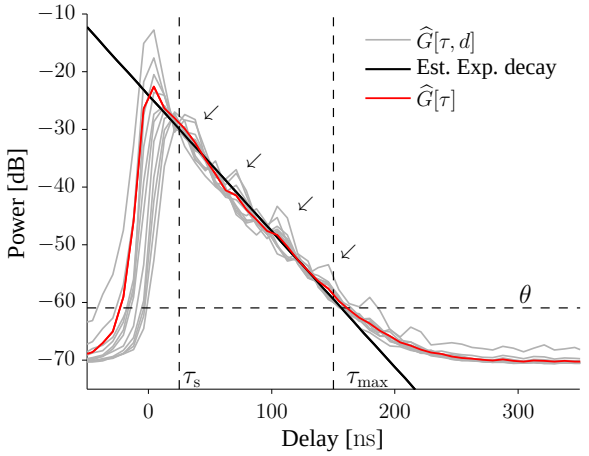

Fig. 5. Spatially averaged delay power spectrum $\widehat{G}[\tau]$ and $\widehat{G}[\tau, d]$ [6]. For displaying convenience $\widehat{G}[\tau, d]$ is shown for every second distance section. The straight line depicts an exponentially decaying function with decay constant $\widehat{T} = 18.4\mathrm{ns}$ corresponding to $-0.24\mathrm{dB/ns}$. The arrows indicate the delays of the reoccurring peaks in the spectrum estimates (see also Fig. 6), caused by propagation paths with multiple reflections between the metallic whiteboard and the windows.

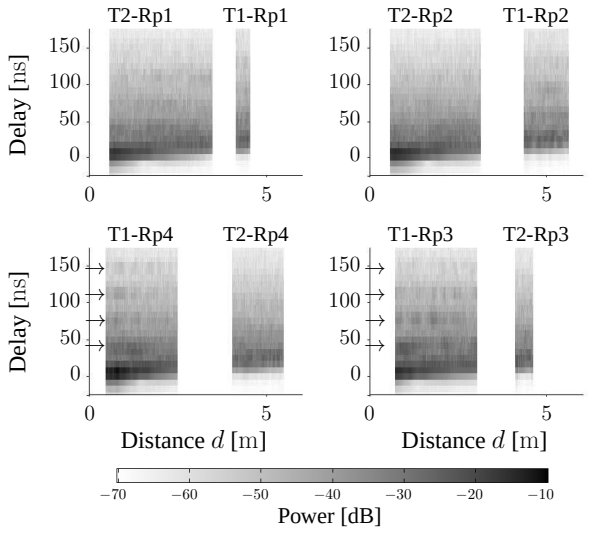

Fig. 6. Estimates of the delay power spectrum (see (36)) for room R4 versus transmitter-receiver distance. Results are shown for the receiver positions Rp1 to Rp4 and the tracks T1 and T2. The arrows on the lower panel indicate the delays of the reoccurring peaks in the spectrum estimates (see also Fig. 5), caused by propagation paths with multiple reflections between the metallic whiteboard and the windows.

via cables throughout the measurements. The used transmit antenna [35] is omni-directional with 3 dBi gain. The receiver was equipped with a uniform circular array of $M = 8$ monopoles with diameter 75.18 mm. These monopoles were connected to the receiver via a multiplexer. The multiplexer and the cables connecting the receive antennas to it introduce an additional known delay τ_{mux} which could not be removed in the calibration process but can be accounted for during the post-processing. In a measurement cycle T_{C} all eight channel frequency responses are sequentially measured. The sounder was operating in "burst" mode. In each burst C consecutive measurement cycles are performed. The duration of one burst is $T_{\mathrm{B}} = C \cdot T_{\mathrm{C}}$. In between bursts, the sounder pauses for data storage, resulting in the burst repetition time T_{BR}. The setting of the sounder selected for the measurement campaign is reported in Table II.

Channel measurements were obtained for seven fixed receive antenna array locations (Rp1 to Rp7), shown in Fig. 4a. The transmit antenna was mounted on a model train which moved on three tracks (T1 to T3). The positions Rp1 to Rp7 and the trajectories along the tracks were measured with a tachymeter. The odometer of the model train was connected to the channel sounder to record the traveled distance during the movement. For each receiver position the frequency response was measured while the transmitter was moving along a track. The transmitter moved with a constant speed of approximately 0.07 m/s. According to the setting of T_{B} in Table II this corresponds to a movement of 0.005 wavelengths within a burst. Over this distance the channel response can be considered quasi-static. Between two consecutive bursts (T_{BR}), the transmitter moved 1/6.3 wavelengths.

[6]The spatially averaged delay power spectrum $\widehat{G}[\tau]$ is obtained as the average of $\widehat{G}_{r,p,q}[\tau]$ over all transmitter and receiver positions in room R4. For a given distance d, $\widehat{G}[\tau, d]$ is the spatial average of $\widehat{G}_{r,p,q}[\tau]$ over all transmitter and receiver positions with distance belonging to a section centered around d. Distance sections have a length of 4 wavelengths and stretch over the full range of transmitter-receiver distances.

B. Post-processing of the Measurement Data

We apply the following post-processing procedure on the experimental data. The measured frequency responses are averaged over all cycles in each burst to reduce noise. The resulting averaged frequency response is denoted by $\widehat{H}_{m,r,p,q}[f]$ where m is the index of the receive array element at receiver position index r and at transmitter position p along track q. The brackets around f indicate that the frequency variable has been discretized, due to the measurement process. We estimate the path gain of the channel for the transmitter at position p along track q and the receiver at position r as

$$\widehat{G}_{r,p,q} = \frac{1}{M} \sum_{m=1}^{M} \frac{1}{B} \sum_{i=0}^{N_c-1} |\widehat{H}_{m,r,p,q}[i\Delta_f]|^2 \Delta_f. \tag{34}$$

To estimate the delay power spectrum of the said channel we first average the modified periodograms of $\widehat{H}_{m,r,p,q}[f]$, $m = 1, \ldots, M$:

$$\widehat{G}'_{r,p,q}[\tau] = \frac{1}{M} \sum_{m=1}^{M} \left| \mathrm{IDFT}\left\{ \widehat{H}_{m,r,p,q}[f]\, W[f] \right\}[\tau] \right|^2. \tag{35}$$

In this expression $\mathrm{IDFT}\{\cdot\}$ is the inverse discrete Fourier transform of the function given as an argument and $W[f]$ denotes a Hann window applied to suppress sidelobes. We obtain the estimated delay power spectrum by shifting (35) ahead by τ_{mux} to remove the additional delay due to the cables and multiplexer:

$$\widehat{G}_{r,p,q}[\tau] = \widehat{G}'_{r,p,q}[\tau + \tau_{\mathrm{mux}}]. \tag{36}$$

Note that, the positions at which the measurements used in the average in (35) were taken only span one wavelength. Therefore the estimate $\widehat{G}_{r,p,q}[\tau]$ undergoes large scale fading.

The mean delay estimate is obtained by numerical integration of (15) with $G(\tau, d)$ replaced by a truncated version of $\widehat{G}_{r,p,q}[\tau]$. Indeed, to reduce the effect of noise we use only the parts of $\widehat{G}_{r,p,q}[\tau]$ exceeding a threshold θ; see Fig. 5. The rms delay spread and higher order moments are estimated similarly, e.g. using (19). The limited bandwidth of the measurement system affects the estimation of the rms delay spread of the channel. We compensate for this by subtracting the second central moment of the inverse Fourier transform of $W[f]$ from the second central moment of the truncated version of $\widehat{G}_{r,p,q}[\tau]$.

By applying the above post-processing to any of the average frequency responses gathered from the measurements in room R3 and R4 we obtain data sets denoted as $\mathcal{D}3$ and $\mathcal{D}4$, respectively. These data sets are used for the validation of the model. Each set consists of estimates of the delay power spectrum, path gain, mean delay, rms delay spread, higher moments, the kurtosis and the corresponding transmitter-receiver distances inside the room.

IV. Validation of the Proposed Model

The estimated delay power spectra in Fig. 5 confirm the observations from [9]–[11], [15] that: i) the reverberant tails coincide and ii) the primary component vanishes for large distances. Thus, the assumptions underlying the model (2)–(4) of the delay power spectrum are fulfilled. Fig. 6 shows the estimates of the delay power spectrum versus transmitter-receiver distance for room R4. The estimates are shown for distances obtained from receiver positions Rp1 to Rp4 and all transmitter locations along the two tracks. We apply no spatial averaging within distance sections as done to obtain the delay power spectrum estimates depicted in Fig. 5. The similarity of the reverberant tails is apparent for the four receiver positions and all transmitter locations along the two tracks.

We now validate the model (2)–(4) by checking its predictions of path gain, mean delay, rms delay spread and kurtosis. To this end, we split the data set $\mathcal{D}4$ into a fitting set $\mathcal{D}4_F$ and a validation set $\mathcal{D}4_V$. We let $\mathcal{D}4_F$ be the data set for receiver positions Rp1 to Rp4 and $\mathcal{D}4_V$ be the data for receiver position Rp5 in room R4. Notice that $\mathcal{D}4 = \mathcal{D}4_F \bigcup \mathcal{D}4_V$, and $\mathcal{D}4_F \bigcap \mathcal{D}4_V = \emptyset$. Similarly $\mathcal{D}3$ is split into $\mathcal{D}3_F$ and $\mathcal{D}3_V$ corresponding to receiver positions Rp6 and Rp7, respectively, in room R3.

For $\mathcal{D}4$ we fit the model (2)–(4) by first estimating T from the estimated delay power spectra and afterwards estimating the remaining model parameters by non-linear least squares fitting of (8) to the scatter plot of estimated path gains versus distance. The reverberation time is the least square estimate of the slope of the estimated log delay power spectra within the delay range $\tau_\mathrm{s} \leq \tau \leq \tau_\mathrm{max}$ as indicated in Fig. 5. The value of τ_s is chosen to reduce the influence of the primary component on the slope estimate. We chose τ_s to be the delay sample closest to the propagation time between transmitter and receiver at the maximum transmitter-receiver distance occurring in $\mathcal{D}4$ plus one pulse duration. The value of τ_max is the largest delay sample such that $\widehat{G}_{r,p,q}[\tau]$ exceeds the threshold θ. For $\mathcal{D}4_F$, we obtain in this way $\widehat{T} = 18.4\,\mathrm{ns}$.

TABLE III
Parameter estimates and Root Mean Squared Errors (RMSEs) of path gains for room R3 and R4.

Model	Parameter estimates				RMSE† [dB]	
	$\widehat{G}_0$	$\widehat{n}$	$\widehat{R}_0$	$\widehat{T}$ [ns]	Fit to $\mathcal{D}(\cdot)_F$	Pred. of $\mathcal{D}(\cdot)_V$
One-slope R4	$1.14 \cdot 10^{-5}$	1.13	—	—	1.27	1.33
Proposed R4	$6.85 \cdot 10^{-6}$	2.2	0.35	18.4	1.17	1
One-slope R3	$9.28 \cdot 10^{-6}$	1.27	—	—	0.66	0.73
Proposed R3	$5.06 \cdot 10^{-6}$	2.67	0.41	16.7	0.5	0.65

Reverberation region R4: $\widehat{d}_\mathrm{rl} = 1.39\,\mathrm{m}$, $\widehat{d}_\mathrm{ru} = 42\,\mathrm{m}$, $\widehat{d}_\mathrm{max} = 12\,\mathrm{m}$.
Reverberation region R3: $\widehat{d}_\mathrm{rl} = 1.16\,\mathrm{m}$, $\widehat{d}_\mathrm{ru} = 52\,\mathrm{m}$, $\widehat{d}_\mathrm{max} = 13.4\,\mathrm{m}$.
† The path gain values in dB are used to obtain the RMSE.

We obtain the same value for $\mathcal{D}4_V$. The parameters G_0, n and R_0 are estimated by fitting the path gain model (8) with reference distance $d_0 = 1\,\mathrm{m}$ to the scatter plot of estimated path gain values versus distance for $\mathcal{D}4_F$. We use a non-linear least squares estimator [36] with $\widehat{T}$ as input. This procedure is repeated for $\mathcal{D}3$. The estimates of T for $\mathcal{D}3$ and $\mathcal{D}4$ are listed in Table III. For comparison we also report the estimates of the parameters of the one-slope model obtained via linear least squares fitting.

The ability of the two models to fit and predict the experimental power values in dB is evaluated by comparing their respective root mean squared errors (RMSEs), which are reported in Table III. The model (2)–(4) yields a lower RMSE for $\mathcal{D}4_F$ and $\mathcal{D}3_F$ than the one-slope model. This is expected since the former model contains more parameters than the latter and includes it as a special case. Furthermore, when comparing the RMSE values for the fitting and validation data in room R4, we see that the one-slope model yields a higher value for the validation data, while the proposed model achieves a lower value. Compared to the one-slope model, our model not only fits the data better, but also yields a better prediction, thus justifying its added complexity. The reason for the proposed model's superior prediction ability appears from Fig. 7a: it provides a close fit at all distances whereas the one-slope model shows its best fit for the range of distances corresponding to the bulk of observations. Fitting the one-slope model to $\mathcal{D}4_F$, where the bulk of observations is at distances larger than $4\,\mathrm{m}$ leads to larger deviations at short distances. This is apparent by swapping the roles of the data sets $\mathcal{D}4_V$ and $\mathcal{D}4_F$: In this case, the one-slope model shows poor prediction for $d > 3\,\mathrm{m}$. A similar effect can be observed for room R3 in Fig. 8a; however, the fit is worse at short distances as the bulk of samples covers larger distances ($d > 1.1\,\mathrm{m}$) in $\mathcal{D}3_V$.

The proposed model allows for the prediction of wideband parameters such as mean delay, rms delay spread and kurtosis. The prediction values are compared to estimates obtained from $\mathcal{D}4$ and $\mathcal{D}3$ in Fig. 7 and Fig. 8, respectively. We observe a good general agreement in trend between the predicted parameters and the estimates computed from both fitting and validation data sets for room R3 and R4. This agreement is remarkable considering that the model parameters are obtained from fitting the path gain model, but not the wideband parameters.

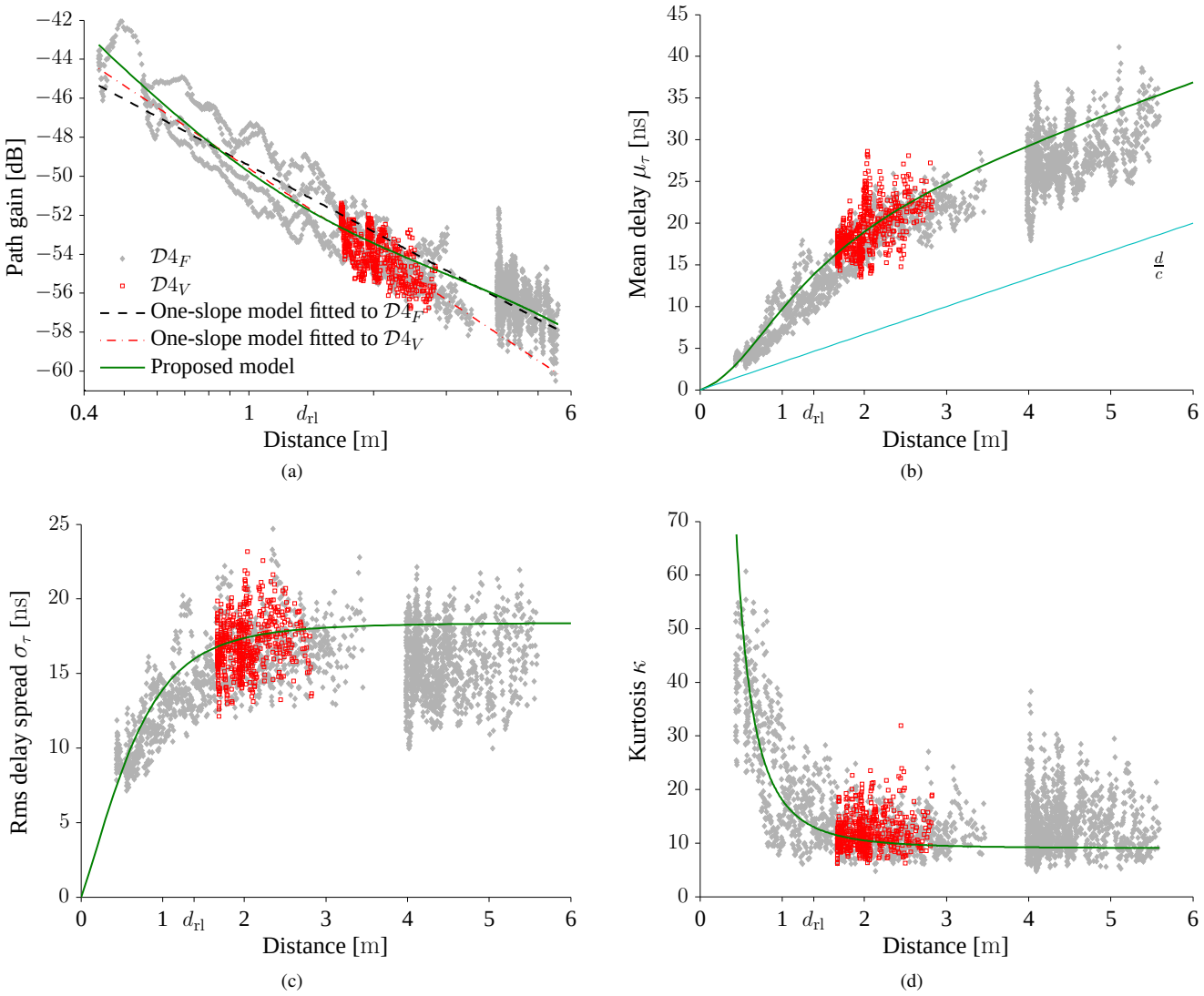

Fig. 7. Experimental results for $\mathcal{D}4_F$ and $\mathcal{D}4_V$ together with the model predictions (solid lines) using the reported parameters in Table III. The dashed and dashed dotted lines in (a) correspond to the standard path gain model. For reference we also plot the line corresponding to $\frac{d}{c}$ in (b).

We quantify the agreement for $\mathcal{D}4$ by comparison of predictions obtained with the secondary models of the wideband parameters with spatial averages of the corresponding estimates. We compute the average of mean excess delay $\mu_\tau(d) - \frac{d}{c}$, rms delay spread and kurtosis evaluated at the same set of distances exceeding 2 m as used for the experimental data. The relative errors between the average values of estimates and the corresponding values predicted by the models for room R4 are 2.4 ns for mean excess delay, 1.9 ns for rms delay spread, and 3.4 for the kurtosis. Using the values from model prediction, the relative errors amount to 16%, 11% and 35%, respectively. The average values of estimates are observed to be close to the model predictions, especially when considering that $\widehat{T}$ varies by ± 1 ns for different settings of τ_{s} and/or $\tau_{\max}$. We remark that by using the procedure described in [17], which uses the rms delay spread to compute an estimate of $\widehat{T}$, we can obtain a better agreement of the rms delay spread and mean delay. However, with this "fine tuning" of the model one uses more data for the fitting procedure and thus discards the rms delay spread for prediction/validation purposes. In this contribution we focus on the model validation and therefore we use for model fitting the estimate $\widehat{T}$ obtained from the slope of the estimated delay power spectrum.

The variation of the estimates of mean delay, rms delay spread and kurtosis around their respective model prediction is occasionally large. This is caused by small and large scale fading, which is not entirely removed in the estimated delay power spectra used compute the parameter estimates. Additionally, for some transmitter locations we observe strong peaks with a delay separation of approximately 35 ns, e.g. indicated with arrows in the lower panel of Fig. 6 and Fig. 5. These peaks originate from propagation paths that are generated by multiple reflections between the metallic whiteboard and the windows. These multiple reflections were identified in [21] as Fabry-Pérot modes.

The truncation of the delay power spectrum in the post-processing may distort the estimated parameters. To evaluate the relevance of this effect, we modified the proposed model

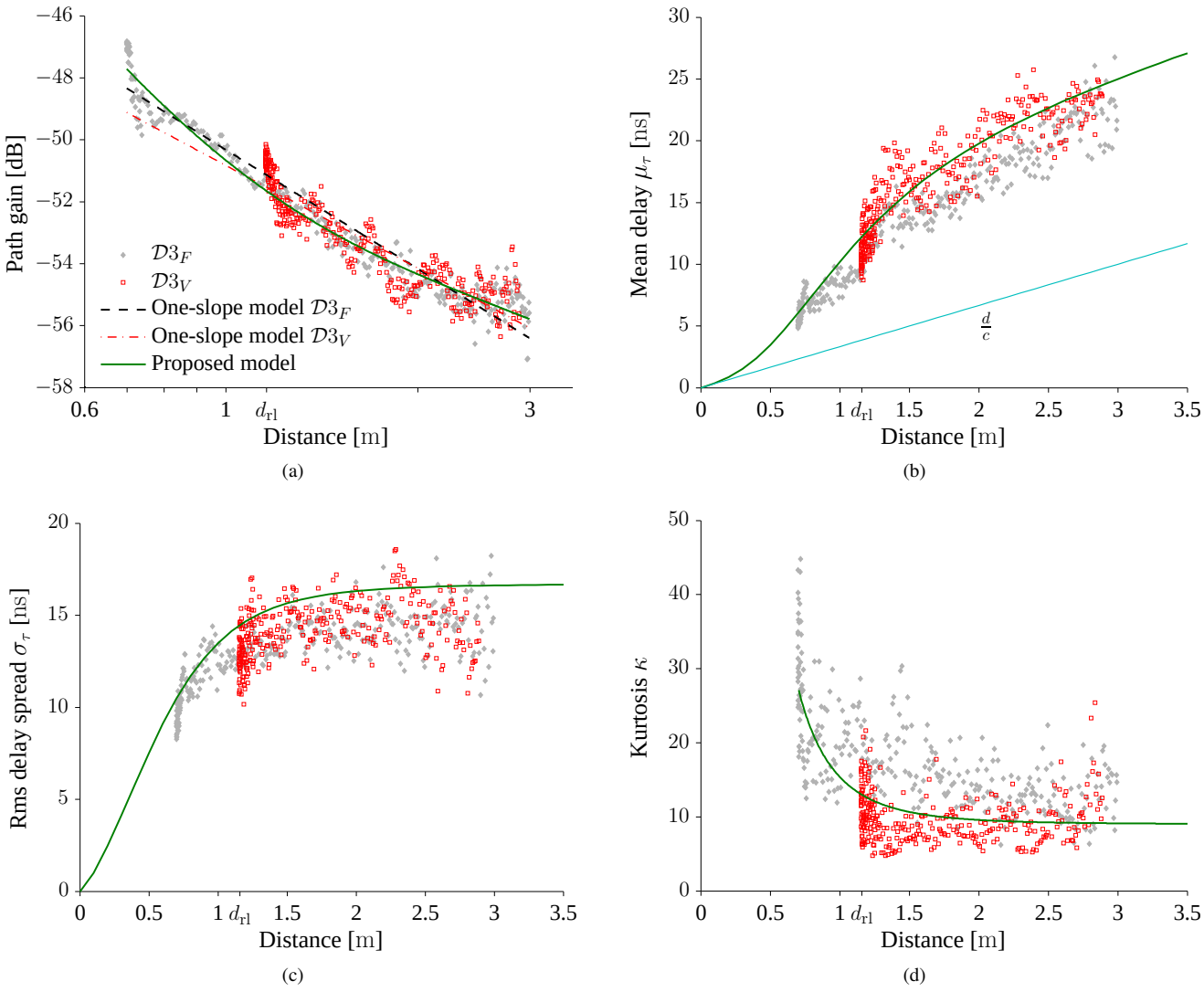

Fig. 8. Experimental results for $\mathcal{D}3_F$ and $\mathcal{D}3_V$ together with the model predictions (solid lines) using the reported parameters in Table III. The dashed and dashed dotted lines in (a) correspond to the one-slope path gain model. For reference we also plot the line corresponding to $\frac{d}{c}$ in (b).

to include the truncation in the delay power spectrum. For the investigated environment and chosen θ this led to no significant changes of the predicted path gain and mean delay. However, in the considered scenario the truncation reduced the predicted rms delay spread by at most 0.5 ns. We also noticed a reduction of the predicted d_{ru}. This effect is, however, of no practical relevance, since the value is still much larger than the length of the diagonal of the room.

A. Model Parameter Estimates

Estimates of the model parameters are listed in Table III. The estimates of the path loss exponent for both rooms ($\widehat{n} = 1.13$ and $\widehat{n} = 1.27$) reported for the one-slope model are slightly below published values obtained from in-room measurement data; see [7] and references therein. The path gain exponent estimate for room R4 computed from $\mathcal{D}4_V$ is $\widehat{n} = 1.41$ which is in the range of values reported in [7]. The measurements used to generate $\mathcal{D}3_V$ were taken within the reverberation region. This explains why the estimate of the path loss exponent is only $\widehat{n} = 1.1$. Path loss exponents below two are traditionally attributed to wave guiding effects. However, considering the room dimensions, a reverberation phenomenon seems to be a more plausible reason of the low values.

For room R4, the estimated path gain exponent $\widehat{n} = 2.2$ of the proposed model's primary component is close to the exponent of free-space propagation. The value $\widehat{R}_0 = 0.35$ indicates that at 1 m distance 35% of the total power is contained in the reverberant component and with increasing distance the reverberant component will gain importance. For room R3 we obtain $\widehat{R}_0 = 0.41$, which is even larger than for R4. Thus, the reverberant component in these two rooms significantly contributes to the total path gain.

The estimate of the reverberation time is within the range of values reported in [11], [12], [15], [37], [38]. The estimated reverberation distance $\widehat{d}_{\mathrm{rl}}$ is about one sixth of the maximum possible distance in rooms R3 and R4. This indicates that the reverberant component dominates over the primary component for a large portion of the room. This in turn leads to the low path loss exponents that we also observe. In addition, $\widehat{d}_{\max}$ is

larger than the length of the room diagonal.

V. Examples of Applications

In the following we give two example applications of the proposed delay power spectrum model. The first example is a distance dependent description of the Rice K-factor and the second is a model to generate discrete-time impulse responses.

A. Example 1: Modeling the Rice Factor as a Function of Distance

In the literature the amplitude of the narrowband radio channel response is often modeled as a Rice distributed random variable. This random variable can be characterized by the Rice K-factor which was observed in [11], [13], [39] to vary with distance. In the following we utilize the model of the delay power spectrum to model the K-factor.

The narrowband channel response is obtained as:

$$h(d) = \int h(\tau, d)\,\mathrm{d}\tau = h_{\mathrm{pri}}(d) + h_{\mathrm{rev}}(d). \tag{37}$$

The primary component $h_{\mathrm{pri}}(d)$ consists of the contributions of the direct line of sight path and possible first order reflections, whereas the reverberant component $h_{\mathrm{rev}}(d)$ is the sum of many higher order reflections. For fixed d, we assume the two components to be independent and normal distributed random variables. More specifically,

$$h_{\mathrm{pri}}(d) \sim \mathcal{CN}\{\mu_{\mathrm{pri}}(d), G_{\mathrm{pri}}(d) - |\mu_{\mathrm{pri}}(d)|^2\}, \tag{38}$$

$$h_{\mathrm{rev}}(d) \sim \mathcal{CN}\{0, G_{\mathrm{rev}}(d)\}, \tag{39}$$

where $\mathcal{CN}\{\,\cdot\,,\,\cdot\,\}$ denotes a circular symmetric complex Normal distribution. Hence, $|h_{\mathrm{pri}}(d)|$ and $|h_{\mathrm{rev}}(d)|$ are respectively Rice and Rayleigh random variables. We assume the K-factor of the primary component to be independent of distance:

$$K_{\mathrm{p}} = \frac{|\mu_{\mathrm{pri}}(d)|^2}{G_{\mathrm{pri}}(d) - |\mu_{\mathrm{pri}}(d)|^2}. \tag{40}$$

Later in this section we will validate this assumption with experimental data. Consequently, $|h(d)| = |h_{\mathrm{pri}}(d) + h_{\mathrm{rev}}(d)|$ is Rice distributed with K-factor

$$K(d) = \frac{|\mu_{\mathrm{pri}}(d)|^2}{G_{\mathrm{pri}}(d) + G_{\mathrm{rev}}(d) - |\mu_{\mathrm{pri}}(d)|^2}. \tag{41}$$

Making use of (40) and (9) we obtain

$$K(d) = \frac{1 - R(d)}{\frac{1}{K_{\mathrm{p}}} + R(d)}. \tag{42}$$

Fig. 9a reports (42). Notice that the distance dependency in (42) stems solely from the distance dependent reverberation ratio. We observe that for the chosen parameter settings the graphs of $K(d)$ are close to that of its limit for $K_{\mathrm{p}} \to \infty$

$$K_{\infty}(d) = \frac{1 - R(d)}{R(d)} \tag{43}$$

when $K_{\mathrm{p}} > 20$. This special case corresponds to a non-fading primary component, for instance contributed by the sole propagation path via line of sight and no first order reflection. Further properties of $K(d)$ are stated in Appendix C.

TABLE IV
Estimates of K_p for room R3 and R4.

	R4 T1	R4 T2	R3 Rp6	R3 Rp7
$\widehat{K}_p$ (fitting (42))	1.7	52	1.59×10^5	1.59×10^5
$\widetilde{K}_p$ (Appendix D)	0 . . . 2	10 . . . 18	—	—

The proposed model of the Rice factor can be related to similar models presented in [39] and [13]. The derivation of the model proposed in [39] relies on the following steps: i) assume $K_{\mathrm{p}} = \infty$, ii) approximate $G_{\mathrm{rev}}(d)$ with a distance independent term G_{rev} and iii) use the definition of the reverberation distance to obtain $G_{\mathrm{rev}} = G_{\mathrm{pri}}(d_{\mathrm{rl}})$. Inserting the latter term into (43) via (7) one obtains the model $K(d) = (d_{\mathrm{rl}}/d)^n$ in [39]. Note that in [39] n and d_{rl} are observed to be frequency dependent. The approximation ii) may be sufficient when the reverberation time is large, such as in reverberation chambers. However, in-room environments found in office or residential buildings have typically much lower reverberation times and therefore the distance dependent onset of the reverberant component cannot be neglected. The model in [13] is similar to that in [39] except that i) it includes the directivity of the transmit antenna, ii) the expression for the effective radius (reverberation distance) obtained from reverberation theory is not inserted, and iii) $n = 2$ is used.

In Fig. 9b and Fig. 9c we compare estimates of K to the model (42). These estimates are obtained from measurements made in room R3 and R4 as described in Appendix D. We obtain an estimate of K_{p}, denoted by $\widehat{K}_{\mathrm{p}}$, by fitting (42) to the estimates of K using the parameters reported in Table III. The obtained values of $\widehat{K}_{\mathrm{p}}$ are reported in Table IV. The estimates of K and the model (42) agree well in trend, except for a few outliers at approximately $4\,\mathrm{m}$ on track T2 in R4 where the concentration of estimates is high. Line-of-sight conditions are fulfilled at all times: However, we observe two distinct behaviors corresponding to either a large or small $\widehat{K}_p$. A small value indicates that the primary component fades, which was not considered in [13], [39].

We investigate the observed differences in the values of $\widehat{K}_{\mathrm{p}}$ for track T1 and T2 in room R4. The analysis of the tail of the impulse responses confirms that $|h_{\mathrm{rev}}(d)|$ is Rayleigh distributed with almost identical parameters for tracks T1 and T2. We obtain estimates of K_{p} from $|h_{\mathrm{pri}}(d)|$ directly using a different estimation procedure detailed in Appendix D. This estimator relies on the fact that the wideband data are available and returns the estimates $\widetilde{K}_{\mathrm{p}}$ for distances up to the reverberation distance. Values of $\widetilde{K}_{\mathrm{p}}$ are reported in Table IV. In neither track, a distance dependence of $\widetilde{K}_{\mathrm{p}}$ is observed. Thus, the assumption made in (40) is appropriate for our measurements. The values of $\widetilde{K}_{\mathrm{p}}$ are close to $\widehat{K}_{\mathrm{p}}$ obtained from model fitting for track T1, see Table IV. The difference between $\widetilde{K}_{\mathrm{p}}$ and $\widehat{K}_{\mathrm{p}}$ for track T2 may seem large, however, the graphs of $K(d)$ for K_p set equal to these estimates are close to each other in the used distance range as shown in Fig. 9b. More importantly, we observe that the $\widetilde{K}_{\mathrm{p}}$ values for the two tracks diverge by one order of magnitude. This indicates that the distinct behavior of $K(d)$ for the two tracks is caused by differences in the primary components. We do not have enough

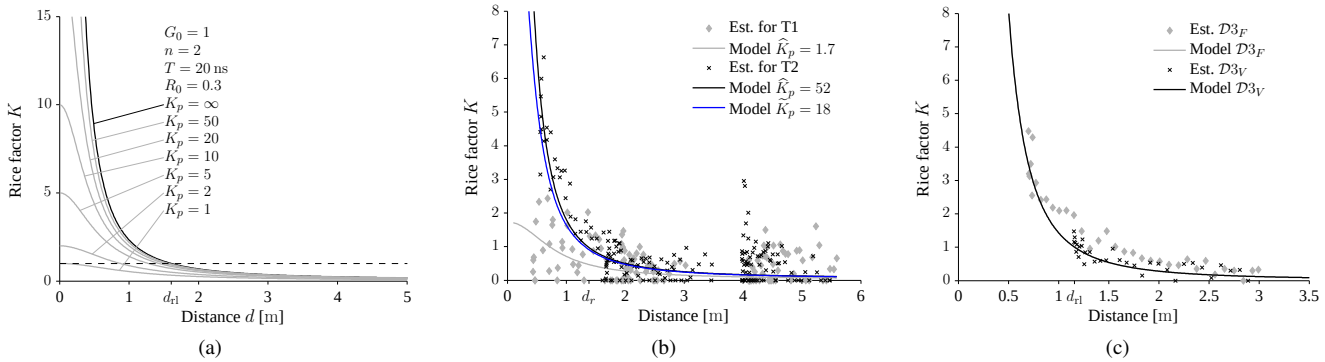

(a) (b) (c)

Fig. 9. Graphs of the proposed Rice K-factor model (42) with K_p as a parameter are shown in (a). Estimated K-factors for measurement set $\mathcal{D}4_F$ in room R4 are shown individually for track T1 and T2 in (b). The graphs of (42) for these estimates are included too. The graphs of (42) for $\widehat{K}_p = 52$, $\widehat{K}_p = 18$, and $K_p = \infty$ are practically the same for the considered distance range. Estimated K-factors for the measurement sets $\mathcal{D}3_F$ and $\mathcal{D}3_V$ in room R3 are shown in (c). The graphs of (42) are also included. For the two sets the curves fall on top of each other and are practically identical to $K_p = \infty$.

data outside the reverberation region to estimate $K_{\rm p}$ for room R3.

The deviation between the estimates of $K_{\rm p}$ obtained for track T1 and T2 may be attributed to the dissimilarity of the near surroundings of the transmitter and the receiver. Track T1 runs closely along a metallic whiteboard leading to a strong first order reflection, resulting in fading of the primary component and thus in small $K_{\rm p}$ values. Track T2 runs along windows with metallic frames and metal coated glass. We expect the metal coated glass to have a lower reflection coefficient than the whiteboard, and thus $K_{\rm p}$ to be high. In room R3, the track and the receiver positions are in the center in the room. This leads at short transmitter-receiver distances to larger differences between the propagation lengths of the direct path and first order reflection paths, which in turn leads to a higher $K_{\rm p}$.

In conclusion, for modeling purposes the assumption $K_{\rm p} = \infty$ holds if the first order reflections are weak. Conversely, if strong first order reflections are present $K_{\rm p}$ should be chosen close to unity.

B. Example 2: Model for the Discrete-time Channel Impulse Response

This example is inspired from [40], where the idea of a discrete-time model based on reverberation theory is outlined. We obtain the discrete-time model by use of (2)–(4) and (42). At distance d the sampled impulse response of a bandlimited channel is modeled as a sequence $\{h[m]\}$ of independent random variables indexed by m. The sample times are chosen as $m\Delta_\tau + d/c$, thus the reference at $m = 0$ of the discrete-time grid is d/c. The random variables in $\{h[m]\}$ are defined as follows:

$$h[m] \sim \begin{cases} \mathcal{CN}(\mu[m], \sigma^2[m]), & m = 0, 1, 2, \dots \\ 0, & m < 0. \end{cases} \tag{44}$$

We impose the equality

$$\mathrm{E}[|h[m]|^2]\, \Delta_\tau = \int_{(m-\frac{1}{2})\,\Delta_\tau + \frac{d}{c}}^{(m+\frac{1}{2})\,\Delta_\tau + \frac{d}{c}} G(\tau, d)\, \mathrm{d}\tau\,. \tag{45}$$

We select $|\mu[m]|$ for $m = 0, 1, 2, \dots$ such that the K-factor of $|\sum_m h[m]|$ equals $K(d)$ in (42). Similarly to (39), we assume $|\mu[m]| = 0$ for $m > 0$. Consequently by (45),

$$|\mu[0]|^2 = \frac{\frac{1}{\Delta_\tau} G(d)\, K(d)}{1 + K(d)}. \tag{46}$$

Using (42) and (8) we obtain $|\mu[0]|$ in

$$\mu[0] = \sqrt{\frac{G_0 d_0^n}{\Delta_\tau d^n \left(1 + \frac{1}{K_{\rm p}}\right)}}\, e^{-j\phi}, \tag{47}$$

where $j = \sqrt{-1}$ and the random phase ϕ is uniformly distributed on $[0, 2\pi)$. The variance of $h[m]$ has the form

$$\sigma^2[m] = \begin{cases} \frac{G_0}{\Delta_\tau} \left(\frac{\left(\frac{d_0}{d}\right)^n}{1+K_{\rm p}} + \frac{R_0}{1-R_0} e^{\frac{d_0 - d}{c\,T}} \left(1 - e^{-\frac{\Delta_\tau}{2\,T}}\right) \right), & m = 0 \\ \frac{2\,G_0}{\Delta_\tau} \frac{R_0}{1-R_0} e^{\frac{d_0 - d}{c\,T} - \frac{m\Delta_\tau}{T}} \sinh(\frac{\Delta_\tau}{2\,T}), & m > 0. \end{cases} \tag{48}$$

The sampling interval Δ_τ should be chosen such that the differences between the mean delay, rms delay spread and higher moments of the time-discrete model and (16), (20) and (55), respectively, are sufficiently small.

VI. Conclusions

The proposed model of the delay power spectrum of an in-room reverberant channel includes a primary component which follows an inverse distance power law (d^{-n}) and a reverberant component which decays exponentially versus delay and exhibits a distance dependent onset. The proposed model allows for the characterization of path gain, mean delay and rms delay spread, higher order centered moments and the kurtosis value versus distance. We obtained the moment generating function from the analytic expression of the delay power spectrum. The model was validated using measurement data. The prediction of mean delay, rms delay spread and kurtosis agrees with the respective estimates obtained from the measurement data. In the investigated environments the ratio of the reverberant component path gain to the total path gain at the reference distance of 1 m are 0.41 and 0.35 for room R3 and R4, respectively. Hence, the reverberant component is prominent in these environments. The observed reverberation distances are close to 1 m despite the line of

sight condition. Thus for large portions of the room the power of the reverberant component exceeds the primary one. This surprising result may have implications on placing wireless access points in a room, radio localization using the received power, multi-link communication, interference alignment, etc.

The estimated path gain exponent of the primary component in the proposed model is close to the free-space path gain exponent for one data set. Due to its inability to separate the primary component from the reverberant component the one-slope path gain model yields path gain exponents close to 1.1. The one-slope path gain model merely provides a fit of the path gain that blends the contributions from the primary and reverberant component. As a consequence it gives different results for the same environment but different measurement locations.

We presented two applications of the proposed model. The first application is a model for the distance dependent Rice factor. The model is in good agreement with the experimental data. We observe two distinct behaviors, both of which are covered by the model: Either the magnitude of the primary component is practically deterministic, or it is Rayleigh fading. The second application is a discrete-time model which allows for the simulation of impulse responses that depend on distance.

Appendix A
Impulse Response Model Relations

In (1) we define the delay power spectrum as the expectation of the magnitude squared impulse response. We propose to split the delay power spectrum into a primary and reverberant component. In the following we show that under certain assumptions this can be directly mapped into splitting the impulse response into a primary and reverberant component.

$$\begin{aligned} G(\tau,d) &= \mathrm{E}[|h_{\mathrm{pri}}(\tau,d) + h_{\mathrm{rev}}(\tau,d)|^2], && (49)\\ &= \mathrm{E}[|h_{\mathrm{pri}}(\tau,d)|^2] + \mathrm{E}[|h_{\mathrm{rev}}(\tau,d)|^2] \\ &\quad + \mathrm{E}[h_{\mathrm{pri}}(\tau,d)\, h^*_{\mathrm{rev}}(\tau,d)] + \mathrm{E}[h^*_{\mathrm{pri}}(\tau,d)\, h_{\mathrm{rev}}(\tau,d)] && (50)\\ &= G_{\mathrm{pri}}(\tau,d) + G_{\mathrm{rev}}(\tau,d) && (51) \end{aligned}$$

The cross terms $\mathrm{E}[h_{\mathrm{pri}}(\tau,d)\, h^*_{\mathrm{rev}}(\tau,d)]$ and $\mathrm{E}[h^*_{\mathrm{pri}}(\tau,d)\, h_{\mathrm{rev}}(\tau,d)]$ are assumed to be zero.

Appendix B
Derivation of Normalized Centered Moment Generating Function and Kurtosis

The centered moment generating function for (2) reads

$$M(x,d) = \frac{1}{G(d)} \int e^{x(\tau-\mu_\tau(d))} G(\tau,d)\,\mathrm{d}\tau. \qquad (52)$$

The kth order centered moment is obtained by taking the kth derivative of $M(x,d)$ and evaluating at $x=0$. By Leibnitz's rule and evaluating the k^{th} derivative at $x=0$ we have

$$\begin{aligned} \tfrac{\mathrm{d}^k}{\mathrm{d}^k x} M(0,d) = \tfrac{G_0}{G(d)} \Big(\big(\tfrac{d}{c} - \mu_\tau(d)\big)^k \ \big(\tfrac{d_0}{d}\big)^n \\ + \tfrac{R_0}{1-R_0} e^{\frac{d_0-2d+\mu_\tau(d)}{c\,T}} T^k \Gamma\Big(k+1, \tfrac{d-c\mu_\tau(d)}{c\,T}\Big)\Big), \end{aligned} \qquad (53)$$

where $\Gamma(s,x)$ is the upper incomplete gamma function for positive integers s [27]:

$$\Gamma(s,x) = (s-1)!\, e^{-x} \sum_{k=0}^{s-1} \frac{x^k}{k!}. \qquad (54)$$

Inserting for μ_τ the normalized k^{th} centered moment generating function reads

$$\begin{aligned} \mu_k(d) &= \tfrac{\mathrm{d}^k}{\mathrm{d}^k x} M(0,d) \\ &= R(d)\, T^k \Big[(-1)^k \left(R^{k-1}(d) - R^k(d)\right) \\ &\qquad + e^{-R(d)} \Gamma(k+1, -R(d)) \Big]. \end{aligned} \qquad (55)$$

The kurtosis in (23) thus reads

$$\kappa(d) = R^{-1}(d) \frac{R^3(d) - R^4(d) + e^{-R(d)}\Gamma(5,-R(d))}{\left[R(d) - R^2(d) + e^{-R(d)}\Gamma(3,-R(d))\right]^2}. \qquad (56)$$

Appendix C
Further Properties of $K(d)$

From the properties of $R(d)$ (see Section II-B) it follows that

$$\lim_{d\to 0} K(d) = K_{\mathrm{p}}, \qquad \lim_{d\to\infty} K(d) = K_{\mathrm{p}} \qquad (57)$$

and

$$K(d) \geq \frac{1 - R(d_{\max})}{\frac{1}{K_{\mathrm{p}}} + R(d_{\max})} \geq 0. \qquad (58)$$

The special case $K(d_{\max}) = K(d) = 0$ occurs only for $R(d_{\max}) = 1$. At the boundaries of the reverberation region, $R(d_{\mathrm{rl}}) = R(d_{\mathrm{ru}}) = \frac{1}{2}$, and thus

$$K(d_{\mathrm{rl}}) = K(d_{\mathrm{ru}}) = \frac{1}{1 + \frac{2}{K_p}}. \qquad (59)$$

Appendix D
Estimation of $K(d)$ and K_p

For the estimation of the Rice factor $K(d)$ we use the averaged measured frequency response $\widehat{H}_{m,r,p,q}[f]$, see Section III-B. We collect $|\widehat{H}_{m,r,p,q}[f]|$ for all receive antennas m and ten consecutive transmitter positions p on track q, for a specific receiver position r into one data set. We apply the method of moments [41] on this data set to compute an estimate $\widehat{K}$ of the Rice factor. As in [41] we set $\widehat{K} = 0$ when the ratio of the first and second moment of the experimental data is below the theoretical value obtained for $K = 0$. Ten consecutive transmitter positions span approximately 1.6 wavelengths. Accordingly, the transmitter-receiver distance is measured from the center of the circular array to the mean of the ten positions.

The estimation of K_p is done differently: We consider all impulse responses obtained from the eight receive antennas for transmitter positions at a distance to the transmitter within an interval of length $0.15\,\mathrm{m}$. We select in each of these impulse responses the sample at the delay value closest to d/c. These samples are used to estimate K_{p}. To check for distance dependency of K_p we limit the interval length to

$0.15\,\mathrm{m}$. We slide the distance interval in $1\,\mathrm{cm}$ steps from the shortest available transmitter-receiver distance up to the reverberation distance d_{rl} to check for distance dependency of K_p.

REFERENCES

[1] H. Liu, H. Darabi, P. Banerjee, and J. Liu, "Survey of Wireless Indoor Positioning Techniques and Systems," *IEEE Trans. Syst., Man, Cybern. C*, vol. 37, no. 6, pp. 1067–1080, Nov. 2007.

[2] H. Hashemi, "The Indoor Radio Propagation Channel," *Proc. IEEE*, vol. 81, no. 7, pp. 943–968, Jul. 1993.

[3] J. Keenan and A. Motley, "Radio coverage in buildings," in *Br. Telecom Technol. J.*, vol. 8, no. 1, Jan. 1990, pp. 19–24.

[4] E. Damosso, Ed., *Digital mobile radio towards future generation systems: Cost 231 Final Report*. Bruxelles, Belgium: European Commission, 1999.

[5] R. Vaughan and J. B. Andersen, *Channels, Propagation and Antennas for Mobile Communications*. Institution of Engineering and Technology, Feb. 2003.

[6] P. Nobles and F. Halsall, "Indoor Propagation at 17 GHz and 60 GHz – Measurements and Modelling," in *Antennas and Propagation, 1999. IEE National Conference on.*, Mar. 1999, pp. 93–96.

[7] D. Xu, J. Zhang, X. Gao, P. Zhang, and Y. Wu, "Indoor Office Propagation Measurements and Path Loss Models at 5.25 GHz," *Vehicular Technology Conference, 2007. VTC-2007 Fall. 2007 IEEE 66th*, pp. 844–848, 30 Sep. - 3 Oct. 2007.

[8] J. Kunthong and C. Bunting, "A Novel Hybrid Propagation Model," in *IEEE International Symposium Antennas and Propagation Society (APS)*, Jul. 2008, pp. 1–4.

[9] C. Holloway, M. Cotton, and P. McKenna, "A model for predicting the power delay profile characteristics inside a room," *IEEE Trans. Veh. Technol.*, vol. 48, no. 4, pp. 1110–1120, 1999.

[10] R. Rudd, "Statistical prediciton of indoor radio channel impulse response," Ph.D. dissertation, University of Surrey, Sep. 2007.

[11] J. Andersen, J. Nielsen, G. Pedersen, G. Bauch, and J. Herdin, "Room electromagnetics," *IEEE Antennas Propag. Mag.*, vol. 49, no. 2, pp. 27–33, 2007.

[12] J. Nielsen, J. Andersen, G. Pedersen, and M. Pelosi, "On Polarization and Frequency Dependence of Diffuse Indoor Propagation," in *Vehicular Technology Conference, 2011 IEEE 74th*, Sep. 2011.

[13] D. A. Hill, *Electromagnetic Fields in Cavities: Deterministic and Statistical Theories*, ser. IEEE Press Series on Electromagnetic Wave Theory. Piscataway, NJ: Wiley/IEEE Press, 2009.

[14] H. Kuttruff, *Room Acoustics*, 4th ed. London: Taylor & Francis, 2000.

[15] J. Kunisch and J. Pamp, "Measurement Results and Modeling Aspects for the UWB Radio Channel," *Ultra Wideband Systems and Technologies, 2002. Digest of Papers. 2002 IEEE Conf. on*, pp. 19–23, 2002.

[16] V. Erceg, D. Michelson, S. Ghassemzadeh, L. Greenstein, J. Rustako, A.J., P. Guerlain, M. Dennison, R. Roman, D. Barnickel, S. Wang, and R. Miller, "A Model for the Multipath Delay Profile of Fixed Wireless Channels," *IEEE J. Sel. Areas Commun.*, vol. 17, no. 3, pp. 399–410, Mar. 1999.

[17] G. Steinböck, T. Pedersen, B. Fleury, W. Wang, T. Jost, and R. Raulefs, "Model for the Path Loss of In-room Reverberant Channels," in *Vehicular Technology Conference, 2011 IEEE 73rd*, May 2011, pp. 1–5.

[18] R. Bultitude, P. Melancon, H. Zaghloul, G. Morrison, and M. Prokki, "The Dependence of Indoor Radio Channel Multipath Characteristics on Transmit/Receiver Ranges," *IEEE J. Sel. Areas Commun.*, vol. 11, no. 7, pp. 979–990, Sep. 1993.

[19] J. McDonnell, T. Spiller, and T. Wilkinson, "Characterization of the Spatial Distribution of RMS Delay Spread in Indoor LOS Wireless Environments at 5.2 GHz," in *IEEE International Symposium on Personal, Indoor and Mobile Radio Communications (PIMRC)*, vol. 2, Sep. 1998, pp. 621–624.

[20] ITU-R, "Recommendation ITU-R P.1407-4 (10/2009): Multipath propagation and parameterization of its characteristics," Nov. 2009.

[21] R. E. Richardson, "Reverberant Microwave Propagation," Naval Surface Warfare Center, Dahlgreen Division, Tech. Rep. NSWCDD/TR-08/127, Oct. 2008.

[22] J. Khodjaev, Y. Park, and A. Saeed Malik, "Survey of NLOS identification and error mitigation problems in UWB-based positioning algorithms for dense environments," *Annals of Telecommunications*, vol. 65, pp. 301–311, 2010.

[23] L. Mucchi and P. Marcocci, "A new UWB indoor channel identification method," in *Cognitive Radio Oriented Wireless Networks and Communications, 2007. CrownCom 2007. 2nd International Conference on*, Aug. 2007, pp. 58–62.

[24] F. Montorsi, F. Pancaldi, and G. M. Vitetta, "Statistical Characterization and Mitigation of NLOS Bias in UWB Localization Systems," in *NEWCOM++ / COST 2100 Joint Workshop on Wireless Communications*, Paris, France, 1-2 Mar. 2011.

[25] S. Maranò, W. Gifford, H. Wymeersch, and M. Win, "NLOS Identification and Mitigation for Localization Based on UWB Experimental Data," *IEEE J. Sel. Areas Commun.*, vol. 28, no. 7, pp. 1026–1035, Sep. 2010.

[26] Z. Xiao, Y. Hei, Q. Yu, and K. Yi, "A survey on impulse-radio uwb localization," *SCIENCE CHINA Information Sciences*, vol. 53, pp. 1322–1335, 2010.

[27] M. Abramowitz and I. Stegun, *Handbook of mathematical functions: with formulas, graphs, and mathematical tables*. Dover Publications, 1965.

[28] R. M. Corless, G. H. Gonnet, D. E. G. Hare, D. J. Jeffrey, and D. Knuth, "On the Lambert W function," *Advances in Computational Mathematics*, vol. 5, no. Apr., pp. 329–359, 1996.

[29] K. Siwiak, H. Bertoni, and S. Yano, "Relation between multipath and wave propagation attenuation," *IET Electron. Lett.*, vol. 39, no. 1, pp. 142–143, Jan. 2003.

[30] N. Alsindi, B. Alavi, and K. Pahlavan, "Measurement and Modeling of Ultrawideband TOA-Based Ranging in Indoor Multipath Environments," *IEEE Trans. Veh. Commun.*, vol. 58, no. 3, pp. 1046–1058, Mar. 2009.

[31] C. Holloway, D. Hill, J. Ladbury, and G. Koepke, "Requirements for an Effective Reverberation Chamber: Unloaded or Loaded," *IEEE Trans. Electromagn. Compat.*, vol. 48, no. 1, pp. 187–194, Feb. 2006.

[32] M. Awad, K. Wong, and Z. bin Li, "An Integrated Overview of the Open Literature's Empirical Data on the Indoor Radiowave Channel's Delay Properties," *IEEE Trans. Antennas Propag.*, vol. 56, no. 5, pp. 1451–1468, May 2008.

[33] G. Steinböck, T. Pedersen, and W. Wang, "AAU-DLR 2010 Indoor Measurement Campaign – Measurements for Validation of Models for Reverberant and Cooperative Channels," AAU and DLR, Report, 2011.

[34] J. Stephan, Y. Lostanlen, J. Keignart, W. Wang, D. Slock, and F. Kaltenberger, "Measurements of location-dependent channel features," ICT- 217033 WHERE, Deliverable 4.1, Oct. 2008, http://www.ict-where.eu/.

[35] Huber+Suhner, "Datasheet for Sencity Antenna For In-Carriage Wireless Communication, Type: SOA 5600/360/3/20/V_1," Document No. 01.02.1358, May 2007.

[36] Mathworks, "Matlab Curve Fitting Toolbox, Version 1.2.2 (r2008b)," 2008.

[37] A. Bamba, W. Joseph, D. Plets, E. Tanghe, G. Vermeeren, L. Martens, J. Andersen, and J. Nielsen, "Assessment of reverberation time by two measurement systems for room electromagnetics analysis," in *IEEE International Symposium on Antennas and Propagation (APSURSI)*, Jul. 2011, pp. 3113–3116.

[38] J. Kunisch and J. Pamp, "An Ultra-Wideband Space-Variant Multipath Indoor Radio Channel Model," *Proc. IEEE 2006 Int. Conf. on Ultra-Wideband*, pp. 290–294, 16-19 Nov. 2003.

[39] Y. Lustmann and D. Porrat, "Indoor Channel Spectral Statistics, K-Factor and Reverberation Distance," *IEEE Trans. Antennas Propag.*, vol. 58, no. 11, pp. 3685–3692, Nov. 2010.

[40] J. B. Andersen, J. O. Nielsen, G. Bauch, and M. Herdin, "The large office environment - measurement and modeling of the wideband radio channel," in *Proc. IEEE 17th Int. Symposium on Personal, Indoor and Mobile Radio Commun. PIMRC 2006*, 2006, pp. 1–5.

[41] K. K. Talukdar and W. D. Lawing, "Estimation of the parameters of the Rice distribution," *J. Acoust. Soc. Am.*, vol. 89, no. 3, pp. 1193–1197, Mar. 1991.

Gerhard Steinböck received the DI (FH) degree in telecommunications from Technikum Wien, Austria in 1999. From 2000 to 2006, he worked as a R&D engineer at the Austrian Institute of Technology (AIT), Vienna, Austria, contributing among other things in the hard- and software development of a real-time radio channel emulator. Gerhard Steinböck received the M.Sc.E. *(cum laude)* degree in wireless communications from Aalborg University, Denmark, in 2008, where he is currently pursuing a Ph.D. degree in wireless communications. His research interests lie in the area of wireless communications, radio channel modeling, radio channel estimation and sounding, and radio geolocation techniques.

Troels Pedersen received the M.Sc.E. degree in digital communications and the Ph.D. degree in wireless communications from Aalborg University, Denmark, in 2004 and 2009, respectively. Since 2009 he has been with Section Navigation and Communications, at Department of Electronic Systems, Aalborg University, first as assistant professor and since 2012 as associate professor. He received the 'Teacher of the Year 2011' award by the Study Board for Electronics and IT, Aalborg University. In Spring 2012 he was a visiting professor at IETR, University Rennes 1, France. His research interests lie in the area of statistical signal processing and communication theory, including sensor array signal processing, radio geolocation techniques, radio channel modeling, and radio channel sounding.

Bernard H. Fleury (M'97-SM'99) received the Diploma in electrical engineering and in mathematics and the Ph.D. degree in electrical engineering from the Swiss Federal Institute of Technology Zurich (ETHZ), Zurich, Switzerland, in 1978, 1990, and 1990, respectively.

Since 1997, he has been with the Department of Electronic Systems, Aalborg University, Aalborg, Denmark, as a Professor of Communication Theory. He is the Head of the Navigation and Communications Section, which is one of the 11 laboratories of this Department. From 2006 to 2009, he was a Key Researcher with the Telecommunications Research Center Vienna (FTW), Vienna, Austria. During 1978-1985 and 1992-1996, he was a Teaching Assistant and a Senior Research Associate, respectively, with the Communication Technology Laboratory, ETHZ. Between 1988 and 1992, he was a Research Assistant with the Statistical Seminar at ETHZ.

Prof. Fleury's research interests cover numerous aspects within communication theory, signal processing, and machine learning, mainly for wireless communications. His current scientific activities include stochastic modeling and estimation of the radio channel, especially for multiple-input-multiple-output (MIMO) systems operating in harsh conditions, iterative message-passing processing with focus on the design of efficient feasible architectures for wireless receivers, localization techniques in wireless terrestrial systems, and radar signal processing. Prof. Fleury's has authored and coauthored more than 120 publications in these areas. He has developed, with his staff, a high-resolution method for the estimation of radio channel parameters that has found a wide application and has inspired similar estimation techniques both in academia and in industry.

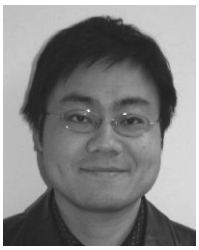

Wei Wang received his Bachelor degree 2003 in the field of communications engineering from University of Wuhan, P. R. China, and Master degree 2006 within the area of digital communications from University of Kiel, Germany. Since 2007 he has been employed as a member of the scientific staff at the institute of Communications and Navigation of German Aerospace Center, where he is pursuing his Doctor degree at the same time. His research interests are channel characteristics analysis and modeling for localization/navigation based on channel measurements, terrestrial radio based positioning/navigation and related topics.

Ronald Raulefs studied electrical engineering at the University of Kaiserslautern, Germany. He attended the University of Edinburgh as an Erasmus student in 1998. He received the Dipl.-Ing. degree from the University of Kaiserslautern, Germany, in 1999 and the Dr.-Ing. (PhD) degree from the University of Erlangen-Nuremberg, Germany, in 2008. Ronald Raulefs initiated and lead the EU FP7 project WHERE and is leading the successor project WHERE2 (www.ict-where2.eu). His current research interests include various aspects of mobile radio communications and positioning, such as space-time signal processing, resource allocation, and cooperative positioning.